Advanced Sliding Mode Control of Heating and Ventilation Unit in a Light Rail Vehicle

Awais SHAH, Deqing HUANG, Tianpeng HUANG, Na QIN*

Southwest Jiaotong University, Xipu, Chengdu, 615305, China
kazmi002@hotmail.com, elehd@home.swjtu.edu.cn,
tphuang@my.swjtu.edu.cn, qinna@home.swjtu.edu.cn (**Corresponding author*)

Abstract: There is a pressing need for energy management with regard to modern rail vehicles, particularly in the case of electric vehicles (EVs), where various forms of energy and loads have to be considered for vehicle running. Air conditioning is an essential factor that ought to be profoundly analysed, as it can account for a significant proportion of electricity demand. This paper considers a lumped-parameter type thermal model of the passenger compartment of a tram in the presence of parametric uncertainties and external disturbances with an optimized heating, ventilating and air conditioning (HVAC) system configuration. To overcome the aforementioned problem, a decoupled sliding mode control (SMC) is designed with the purpose of enabling a lower energy usage and providing the thermal comfort conditions in a tram as an efficient and durable control strategy. The temperature and concentration of carbon dioxide (CO2) are regulated in a desirable way. A proportional, integral and derivative (PID) controller is employed for comparison purposes and for validating the proposed control scheme. According to the findings of this paper, the SMC outperforms the PID controller in terms of fast tracking and steady state for the desired tracking targets.

Keywords: Electric vehicle, HVAC, Robust control, Sliding mode control.

1. Introduction

The metropolitan tram plays a crucial role in reducing the amount of traffic, pollution and urban electricity consumption. Nowadays, modern trains should be outfitted with units for heating, ventilating and air conditioning (HVAC). Up to 30 % of total operating power is utilized by these systems (Pero et al., 2015). In practice, the problem of increasing HVAC energy consumption while also maintaining a healthy indoor environment in the tram section is challenging. Statistical study of data collected from a tram for everyday use in Belgium over a year shows that it is possible to mitigate the use of HVAC units power savings and improve traveller's thermal comfort. By adopting a climate-dependent set point temperature for the indoor air, approximate energy savings varying from 15% to 42% can be achieved (Beusen et al., 2013). The approach and conclusions of the research analysis aimed at determining the power consumption of electric trains often show that on-board auxiliaries have a high energy mitigation ability. Heating has been shown to be responsible for the largest portion of this intake (Lin & Du, 2017; González-Gil et al., 2014). González-Gil et al. (2015), Douglas et al. (2015) and Alfieri et al. (2019) have already emphasized the requirements of techniques and methods for analysing, simulating and optimizing the flow of energy in urban electric rail vehicles.

In urban areas where metropolitan rail is not evolving further it could forfeit its role at the leading edge of financial and equitable urban mobility solutions (Fiori & Marzano, 2018), as intensive research is developing and enhancing new individual electrical transportation modes. Although some alternatives exist (Yang and Wang, 2018) and are utilized in practice (Zhang et al., 2011), automobiles are typically air-conditioned by vapor compression refrigerators. Mastrullo et al. (2016) proposed alternative refrigerant for high-speed trains to reduce environmental emissions and for energy savings. There are three options for modelling HVAC systems, namely: (i) physics-based, (ii) data-driven, and (iii) gray box (Talib et al., 2020). It is possible to apply the same principles to thermal (rail) vehicle models. In the automotive industry, HVAC thermal models have always been state of the art. A thermal model for a car's cabin is developed and implemented in (Marcos et al., 2014) and can be used for HVAC system development and testing. The researchers propose a thermal model based on mathematical formulas for radiation treatment, heat transfer, and thermal inertia. It includes two heat capacities analogous to the design described in the study, namely: (i) cabin's indoor air heat capacity, and (ii) heat capacity of the base component's thermal inertia (dashboard, seats and panels). Nonetheless, without utilizing data, such two-heat capacity numerical values are derived analytically. A similar approach for thermal modelling vehicle cabins under variable ambient conditions is used in (Lee et al., 2015).

The KULI technology kit can be employed in order to test and refine the thermal management process of automotive applications (Anon.,

https://doi.org/10.24846/v30i3y202111

2019). That allows the designer to set up system components and control techniques for optimizing performance, comfort, and quality in service. The initial results for an electric vehicle's air conditioning system, passenger compartment and power electronics are discussed in (Rugh et al., 2011). The researchers tested different concepts for the combination of elements for the process and contrasted the output with a reference model. Lim & Jeong (2019) considered a dedicated outdoor air system for high-speed train cabins with thermoelectric radiant panels that would eliminate difficulties related to air quantity and decrease energy expenditure in operation. It provides outdoor chilled and dry air for ventilation and latent load removal. It is necessary to handle the cooling and heating loads appropriate for use in train cabins. For refrigerated transport systems, conditional parameter (on-off) for temperature control, also employed in (Davies et al., 2017). The researchers incorporated a decentralized template statistical control scheme for refrigeration systems for supermarkets and also took into account regular energy demand fluctuations (Luchini et al., 2019; Krzaczek et al., 2019). The pattern was established by the automotive industry to boost thermal comfort and increase the required energy usage. Muhammad et al. (2018) examined the effect of thermostat rate setting in a car's passenger cabin on fuel efficiency and atmospheric relaxation. The train HVAC Co2 cycle is optimized by multi-objective design (Luger and Rieberer, 2018).

Kim et al. (2018) predicted the thermal comfort response of an individual instead of the average response of a large population, a new personal thermal comfort model was established. Kristanto & Leephakpreeda (2017) recommended mathematical models for a car cabin and the validity of power usage, air quality, and thermal warmth. Since the cost decision in the automotive industry is influenced by thermal comfort in the car, all concerns regarding this comfort are discussed in depth. Bode et al. (2017) examined the impact of an air diffuser's inlet angle on the passenger's thermal comfort in an automobile. The seat cooling function was studied by researchers Veliveli et al. (2017) with a view to enhancing the occupant's thermal satisfaction in automobile environment. The compartment of a train is thermally simulated and tested (Aliahmadipour et al., 2017). In the compartment with and without the presence of the passengers, two conditions namely temperature and velocity comfort criteria, are evaluated. In addition, some modifications are made to enhance the comfort conditions around the passengers. Gao and Yang (2019) designed the optimization tool for energy simulation for urban rail. All critical subsystems that consume energy (traction device and auxiliaries) can be identified using appropriate level of detail models. Operational environments and inner controls model and drive communication between subsystems. Details of mathematical airflow experiments, including water transfer, thermal exposure and travellers' thermal comfort in a train cabin are presented in (Konstantinov and Wagner, 2015). Suárez et al. (2017) proposed an air distribution analysis of computational fluid dynamics (CFD) in a representative railway vehicle equipped with a HVAC system. Techniques and methods for identifying representative HVAC operating conditions in passenger rail vehicles are outlined in (Luger et al., 2016). A fuzzy logic controller is designed in (Beinarts, 2013) for passenger's thermal comfort improvement in electric transport. The new air-conditioning and oxygen supply control system for the running air-conditioned train in Qinghai-Tibet Railway has been introduced in (Li and Wang, 2015). Sliding mode control (SMC), which is also an integral part of this research, was already applied on HVAC system in buildings energy consumption area (Shah et al., 2017, Shah et al., 2018).

Unlike all the referenced sources, the research discussed in this paper contributes specifically the following: a description of HVAC and thermodynamic models for a tram is presented and a controller concept is introduced that takes into account thermal comfort and energy usage. The goal of this study is to define and solve the thermal comfort control problem in rail vehicles by using lowest power consumption while balancing the comfort level. Thermal comfort models are developed for the whole problem for rail vehicles. Two different control strategies namely, (a) Sliding mode control, and (b) PID control are developed and their performance is compared in terms of fast tracking, overshoot and steady state.

The remainder of this paper is structured as follows. Section 2 analyses a tram's thermal behaviour, and it presents setup and linearization of the theoretical model. Section 3 sets forth the control system design, while providing an overview of the application of the controller. Section 4 demonstrates the simulation results obtained and Section 5 represents the conclusion of the proposed study.

2. Methodology

The rail vehicle being studied and simulated is a tram, produced and tended in Chengdu, China, by the CASCO Co. With an unloaded weight of 24 tons, the tram is about 28 m long, 2.2 m wide and 2.8 m high. With an added section of bow and tail, it is divided into three similar sections. Figure 1 displays a general tram block diagram with installed HVAC units on rooftop.

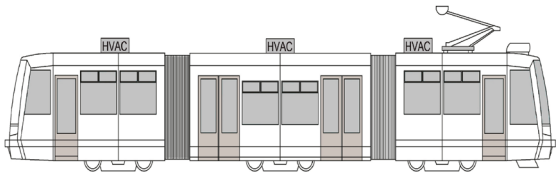

Figure 1. A general schematic illustration of a tram with roof-mounted HVAC units

In each segment there are seventeen seats with five additional seats in the rear section, resulting in a maximum of 54 seats. There is also room for 90 standing commuters. All three primary tram sections have separate HVAC units. Every unit can warm, cool, ventilate, and dehumidify the tram.

The HVAC and controller of tram form a closed-loop control system. The control of actual value of indoor air temperature is the main target. Figure 2 shows the HVAC working in a tram section. A small portion of indoor exhaust air is mixed with outdoor air and then according to control error, air is passed through electric heater or compressor unit according to supply requirement. Different sensors (thermocouples) measure and send data to the controller. By comparing set points and measurements, a control error is produced by the controller. After the control error takes place, the controller then generates the control signal and sends it to the HVAC system. To mitigate the control error, the system correctly controls the air mass flow rate furnished to a section of a tram. The HVAC system requires electrical energy to operate. Different perturbations affect the HVAC systems and tram indoor atmosphere.

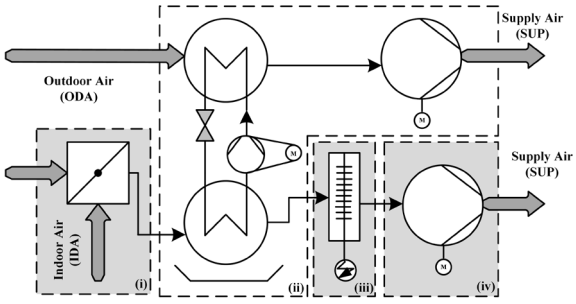

Figure 2. Working of HVAC in a tram section

A thermal dynamic model for the tram is required to explain the air temperature of inside area (T_i) and the carbon dioxide (c_{co2i}) concentration present in the passenger's compartment. Humidity is also an integral element, but the method described here does not include a closed-loop regulation for humidity. The local weather also justifies the possibility to ignore humidity control. Dullinger et al. (2015) and Hofstädter et al., (2017) claim that the train comprises dual thermal structures with two temperatures (the T_i indoor air temperature and the T_v fictional heat capacity of the cabin body) and two energy capacities. The air mass and heat flow in a section of tram is shown in Figure 3.

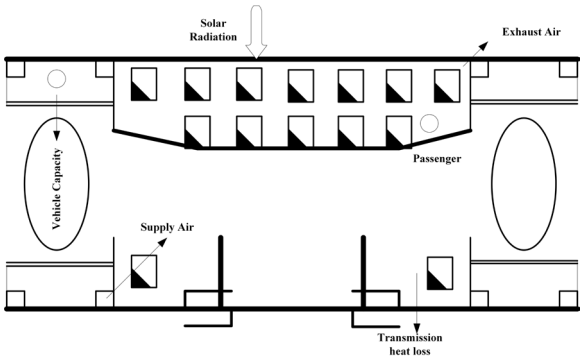

Figure 3. Air mass and heat flow in a section of the tram

For a section of the train, two energy balance equations are expressed as:

$$C_i \frac{dT_i}{dt} = -\dot{H}_l - \dot{H}_v + \dot{H}_{sol} + \dot{H}_p + \dot{E}_s + \dot{E}_e$$

$$C_v \frac{dT_v}{dt} = \dot{H}_v \quad (1)$$

where dT*i* is the indoor temperature of the tram section and C_i is the heat capacity associated with it. The dissipated heat from inside of train to outside environment $\dot{H}_l$ is given by following equation:

$$\dot{H}_l = c_i \cdot S \cdot (T_i - T_v) \quad (2)$$

Transfer of heat from train towards outside air is denoted by $\dot{H}_l$. c_i is heat transfer coefficient of tram. S is uncoiled surface area. The two thermal systems of train T_i and T_v are connected and energy flow between them is given by:

$$\dot{H}_v = c_v (T_i - T_v) \quad (3)$$

The fictitious heat transfer coefficient cv represents flow of heat between two systems. The direct and indirect solar radiations are given by:

$$\dot{H}_{sol} = c_{sol}(t) - \dot{e}_{sol} \quad (4)$$

where, c_{sol} denotes the absorption coefficient and $\dot{e}_{sol}$ represents the intensity of solar radiations. The passengers` dissipated heat is represented by:

$$\dot{H}_p = c_p(t) \cdot n_p \tag{5}$$

The heat quantity produced per person is denoted by $c_p(t)$ and total number of passengers is denoted by n_p. The supply air $\dot{E}_S$ and exhaust air enthalpies $\dot{E}_e$ are given as:

$$\begin{aligned} \dot{E}_s &= \dot{m}_s \cdot C_a \cdot T_s \\ \dot{E}_e &= \dot{m}_s \cdot C_a \cdot T_i \end{aligned} \tag{6}$$

In equation (6), $\dot{m}_s$ and C_a are supply air mass flow and specific heat capacity associated with it, respectively. T_s and T_i are supply air temperature and inside temperature, respectively. By substituting equations (2)-(6) in equation (1) and adding condition for CO_2, the following is obtained:

$$\begin{aligned} C_i \frac{dT_i}{dt} &= c_i(t) \cdot S \cdot (T_o - T_i) - c_v(T_i - T_v) + \dot{m}_s \cdot C_a \\ &\quad \cdot (T_s - T_i) + c_p(t) \cdot n_p + c_{sol}(t) - \dot{e}_{sol} \\ C_v \frac{dT_v}{dt} &= c_v(T_i - T_v) \\ V_i \cdot d_i \frac{dc_{co_2 i}}{dt} &= \dot{m}_s(c_{co_2 s} - c_{co_2 i}) + n_{co_2} \cdot n_p \end{aligned} \tag{7}$$

where T_o is outdoor air temperature, c_{co2i} represents the carbon dioxide concentration inside the train, c_{co2s} represents the supply air carbon dioxide concentration, V_i and d_i are volume and density of inside air, respectively. n_{co2} is the carbon dioxide produced per person. dT_v is the vehicle body temperature. Based on Figure 3, the HVAC supply air temperature and carbon dioxide concentration can be expressed as:

$$\begin{aligned} T_s &= (1 - \gamma_m) \cdot T_i + \gamma_m \cdot T_o + \frac{\dot{P}_c + \dot{P}_h}{C_a \cdot \dot{m}_s} \\ c_{co_2 s} &= (1 - \gamma_m) \cdot c_{co_2 i} + \gamma_m \cdot co \end{aligned} \tag{8}$$

where γ_m is the mixing chamber ratio, P_c and P_h are the powers supplied by compressor and heater, respectively. The outdoor air carbon dioxide amount is *co*. The system presented in equation (7) and equation (8) can be transformed into state space model with the following substitutions:

$$\begin{aligned} &x_1 = T_i, x_2 = T_v, x_3 = c_{co_2 s} \\ &u_1 = \dot{m}_s, u_2 = \dot{P}_c + \dot{P}_h \\ &v_1 = T_o, v_2 = n_p, v_3 = \dot{e}_{sol} \end{aligned} \tag{9}$$

The state space model of system model equation (8) can be represented as:

$$\begin{aligned} \dot{x}_1 &= \frac{1}{C_i}[c_i(t) \cdot S \cdot (v_1 - x_1) - c_v(x_1 - x_2) - u_1 \cdot C_a \cdot x_1 \cdot \gamma_m \\ \dot{x}_2 &= \frac{c_v}{C_v} \cdot (x_1 - x_2) \\ \dot{x}_3 &= \frac{1}{V_i d_i} \cdot \left[(co - x_3) \cdot u_1 \cdot \gamma_m + n_{co_2} \cdot v_2 \right] \end{aligned} \tag{10}$$

For further simplification, equation (10) can be expressed as follows:

$$\begin{aligned} \dot{x}_1 &= f_1(x) + g_1 \cdot u_1 + g_2 \cdot u_2 \\ \dot{x}_2 &= f_2(x_1 - x_2) \\ \dot{x}_3 &= f_3 + g_3(x) \cdot u_1 \end{aligned} \tag{11}$$

where

$$\begin{aligned} &f_1(x) = \frac{1}{C_i}[c_i(t) \cdot S \cdot (v_1 - x_1) - c_v(x_1 - x_2) + c_p(t) \cdot v_2 + c_{sol} \cdot v_3], \\ &g_1 = \frac{1}{C_i}\left[C_a \cdot x_1 \cdot \gamma_m + C_a \cdot \gamma_m \cdot v_1\right], g_2 = \frac{1}{C_i}, \\ &f_2 = \frac{c_v}{C_v}, \\ &f_3 = \frac{n_{co_2} \cdot v_2}{V_i d_i}, g_3(x) = \frac{co - x_3}{V_i d_i}. \end{aligned} \tag{12}$$

3. Controller Design

PID control

The most common sort of controller used in process industries is the PID controller. A PID controller has three parts, namely: (a) Proportional, (b) Integral, and (c) Derivative and their respective gains k_p, k_i and k_d. $e(t)$ is error generated in closed-loop system. As such, the PID controller equation then can be written as:

$$u(t) = k_p \cdot e(t) + k_i \int_a^b e(t)dt + k_d \cdot \frac{de(t)}{dt} \tag{13}$$

In equation (13), *e*(t) is error, $\int_a^b e(t)\,\mathrm{dt}$ is integral of error between a and b limits and *de*(t) is derivative of error.

PID controller parameters tuning

The Ziegler-Nichols approach is utilised to identify the values of PID parameters for the proposed investigation. The Ziegler-Nichols approach relies on tests executed on a control

loop. In order to choose the gains, one must go through the steps below:

- By adjusting $k_i = \infty$ and $k_d = 0$, PID will be transformed into a P controller. Set the value of $k_p = 0$ at first. For the controller, close the loop in programmed mode;
- Increase k_p values unless the indicators in the control system continue to move in the same direction. This k_p value denotes a significant gain, k_{pu};
- Measure the period P_u of the sustained oscillations;
- Calculate the controller parameter estimated values as it is shown in Table 1 and use them in the controller.

Table 1. Design and tuning method for choosing parameters of PID controller

Controller	k_p	k_i	k_d
P controller	$\frac{1}{2}k_{pu}$	∞	0
PI controller	$0.45k_{pu}$	$\frac{1}{2}P_u$	0
PID controller	$0.6k_{pu}$	$\frac{1}{2}P_u$	$\frac{1}{8}P_u$

Advanced sliding mode control

The sliding control technique is a simple approach to robust performance. It is focused on the observation that control of first-order systems (i.e., structures depicted by differential equations of first order) and is much easier than control of general nth-order systems. The sliding controller design offers a deliberate approach to the issue of retaining stability and coherent efficiency against designing imprecisions. It can highlight the entire design cycle by requiring that trade-offs between modelling and efficiency be quantified in a simplistic manner.

Sliding control has been successfully applied to robot swindlers, marine ships, automobile controls and generators, high-performance electric motors and power systems. The control law must be discontinued in sliding surface to account for the existence of design imprecisions with regard to disturbances. Since the design of the related control switches is inherently incomplete (for example, switching is not immediate in action and the value of sliding surface is not understood with absolute precision), chattering occurs (Liu and Wang, 2012). Chattering is not ideal in reality as it requires a high-level control operation and can also cause high-frequency dynamics that is ignored during modelling. It can be avoided by adopting a saturation function in control design. Figure 4 shows the control strategy adopted in this study. From equation (11) it is clear that state x_1 is controlled by input u_2 and state x_3 is manipulated by input u_1. As a result, the MIMO system could be conceived as consisting of two analogous dynamic single-input single-output (SISO) systems.

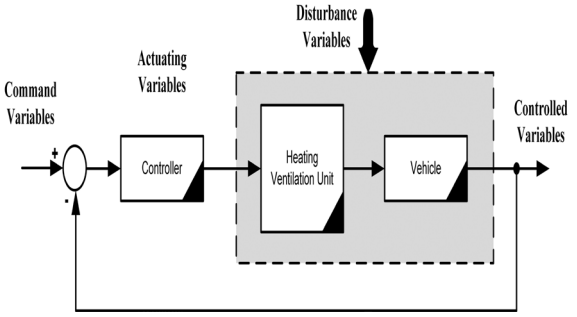

Figure 4. A general block diagram of control scheme

To design control law u_1, x_3 from equation (11) is used. The sliding surface is taken as follows:

$$\dot{s}_3 = -\alpha_1 \int e_3 dt - e_3 \tag{14}$$

where α_1 is a positive constant and $\int e_3 dt$ is tracking error, $e_3 = x_3 - x_{3r}$, in which x_{3r} is the desired trajectory. To operate the system states on the defined sliding surface, it is required that $s_3 = 0$ and $\dot{s}_3 = 0$.

$$\dot{s}_3 = -\dot{e}_3 - \alpha_1 e_3$$

$$\dot{s}_3 = -\alpha_1 e_3 + \dot{x}_{3r} - \dot{x}_3 \tag{15}$$

The equivalent control law can be expressed as:

$$u_{1eq} = \frac{-\alpha_1 e_3 + \dot{x}_{3r} - \dot{x}_3 - f_3^{\triangle}}{g_3^{\triangle}(x)}$$

where, $f_3^{\triangle}$ and are $g_3^{\triangle}(x)$ represents the system dynamics in the absence of uncertainties. The control law to shift state variable on the sliding surface $s_3 = 0$, is given as:

$$u_1 = u_{1eq} + u_{1s} \tag{16}$$

To force the state trajectories to remain on the sliding surface, switching function u_{1s} was used in (17). For the stability analysis, the Lyapunov candidate function (V_3) was chosen as:

$$V_3 = \frac{1}{2}s_3^2 \tag{17}$$

The derivative of (17) must be negative definite to make the control law u1 stable:

$$V_3 = s_3\dot{s}_3 < -\eta\,|\,s_3\,| \quad \eta > 0$$

$$s_3(-\alpha_1 e_3 + \dot{x}_{3r} - \dot{x}_3) = s_3[-\alpha_1 e_3 + \dot{x}_{3r} - (f_3 + g_3(x))u_1] < -\eta_3\,|\,s_3\,|,$$

$$-\alpha_1 e_3 + \dot{x}_{3r} - (f_3 + g_3(x)(u_{1eq} + u_{1s})) < -\eta_3 sgn(s_3),$$

$$\dot{s}_3 = -\alpha_1 e_3 + \dot{x}_{3r} - \dot{x}_3 - f_3 - g_3(x) - \frac{-\alpha_1 e_3 + \dot{x}_{3r} - \dot{x}_3 - f_3^{\triangle}}{g_3^{\triangle}(x)} - g_3(x)u_{1s}, \tag{18}$$

$$\dot{s}_3 = \left(-f_3 + \frac{g_3(x)}{g_3^{\triangle}(x)}f_3^{\triangle}\right) + \left(1 - \frac{g_3(x)}{g_3^{\triangle}(x)}\right) - \left(-\alpha_1 e_3 + \dot{x}_{3r}\right) - g_3(x)u_{1s}.$$

η is positive constant. By considering $u_{1s} = \frac{\gamma_3}{g_3^{\triangle}(x)}sgn(s_3)$, the value of γ_3 needs to be estimated to achieve stability $(\dot{V}_3 < 0)$. Using equation [18], one obtains:

$$\dot{s}_3 = \left(-f_3 + \frac{g_3(x)}{g_3^{\triangle}(x)}f_3^{\triangle}\right) + \left(1 - \frac{g_3(x)}{g_3^{\triangle}(x)}\right) - \left(-\alpha_1 e_3 + \dot{x}_{3r}\right) - g_3(x)\frac{\gamma_3}{g_3^{\triangle}(x)}sgn(s_3),$$

$$\frac{g_3(x)}{g_3^{\triangle}(x)}\dot{s}_3 = \frac{g_3(x)}{g_3^{\triangle}(x)}(-f_3 + f_3^{\triangle}) + \left(\frac{g_3(x)}{g_3^{\triangle}(x)} - 1\right) \times (-\alpha_1 e_3 + \dot{x}_{3r}) - \gamma_3 sgn(s_3), \tag{19}$$

One considers $(-f_3 + f_3^{\triangle}) < F$, F is constant and $\zeta_3 = \frac{g_3 max(x)}{g_3 mix(x)}$, ζ3 is constant, g3(x) is varied between maximum and minimum limits. After substituting these values in equation (19) and further simplifications, the value of γ_3 is obtained as:

$$\gamma_3 \geq \zeta_3 F_3 + (\zeta_3 - 1)\,|\,g_3^{\triangle}(x)\,||\,u_{1eq}\,| + \eta_3\zeta_3 \tag{20}$$

By following the same procedure, u2 and the stability condition γ1 are expressed as:

$$u_2 = u_{2eq} + u_{2s}$$

$$u_{2eq} = \frac{-\alpha_2 e_1 + \dot{x}_{1r} - \dot{x}_1 - f_1^{\triangle}}{g_1^{\triangle}(x)} \tag{21}$$

$$u_{2s} = \frac{\gamma_1}{g_1^{\triangle}(x)}sgn(s_1)$$

$$\gamma_1 \geq \zeta_1 F_1 + (\zeta_1 - 1)\,|\,g_2^{\triangle}(x)\,||\,u_{2eq}\,| + \eta_1\zeta_1. \tag{22}$$

For obtaining appropriate results and performance, the parameters are chosen as:

$$\alpha_1 = 0.00002, \quad \eta_3 = 0.0001, \quad \zeta_3 = 1.01$$

$$\alpha_2 = 0.0005, \quad \eta_1 = 0.00004, \quad \zeta_1 = 1.35$$

4. Results

The effects of the two proposed control system strategies, namely SMC, and PID control are examined in this section. The above-mentioned controls are configured for the marginal HVAC system parameters. Their performance in tracking goals is then assessed and compared. Two practical reference signals are used for controller tracking.

For temperature control inside the tram, the sequence of steps function is used and the ramp-step function is used as the desired set point for CO2 concentration. By keeping thermal comfort in mind, the temperature range is set between 18°C to 23°C and CO2 concentration is between ’1000ppm’ to ’1200ppm’. It should be remembered that in all climatic conditions the built controller can be used effectively.

Figure 5 shows the tracking performance of both SMC and PID controllers. The PID has a big steady-state error when tracking the set point. In its turn SMC produces a small overshoot on sudden step changes, but steady-state and settling time are much lower than those obtained by the PID. The tracking performance of both controllers for CO2 set point is shown in Figure 6. The results show a significantly higher performance of SMC in terms of faster tracking, lower overshoot and steady state, and a quick response to sudden changes. The heater or compressor (heating or cooling mode)

is chosen by the HVAC system itself according to the control error. The power used by HVAC can be calculated based on the control inputs by both controllers. Figure 7(a) shows the control input u_2 (heating or cooling power) from PID and Figure 7(b) shows the same control input from SMC. The PID is using approximately 1100 watt to maintain the inside temperature of 22°C at time 0 to 400 seconds, whereas SMC needs around 200 watts of power to reach the same temperature set point.

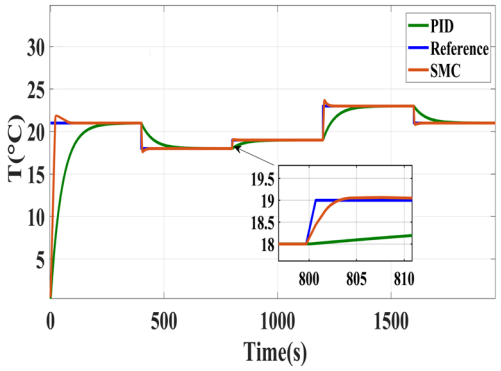

Figure 5. Tracking results of SMC and PID controllers on sequence of steps for temperature set point

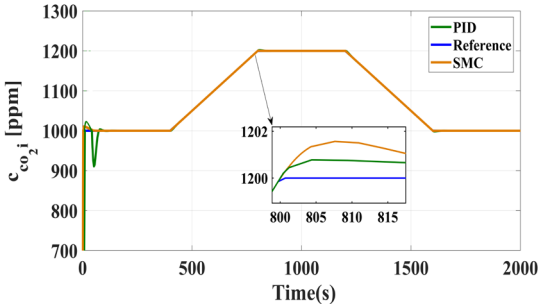

Figure 6. Tracking results of SMC and PID controllers on ramp-step function for $CO_{2\ set\ point}$

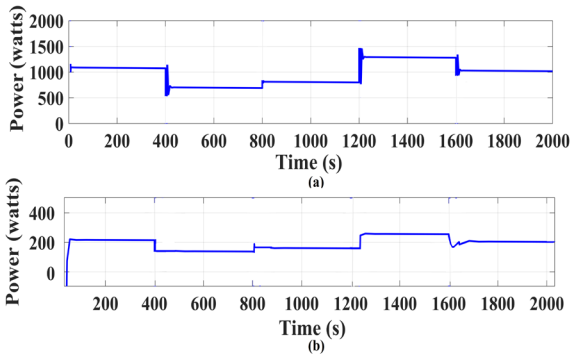

Figure 7. Control input u_2 which also represents the heating power supplied for (a) PID, and (b) SMC

The air supplied by HVAC is controlled by control input u_1. The air mass flow rate of this air consists of fresh air from outside and recirculated air taken from inside. The mixing ratio is adjusted in the mixing chamber according to the set point of Co2. Figure 8(a) and Figure 8(b) show the supply air mass flow rate for the SMC and PID controller respectively.

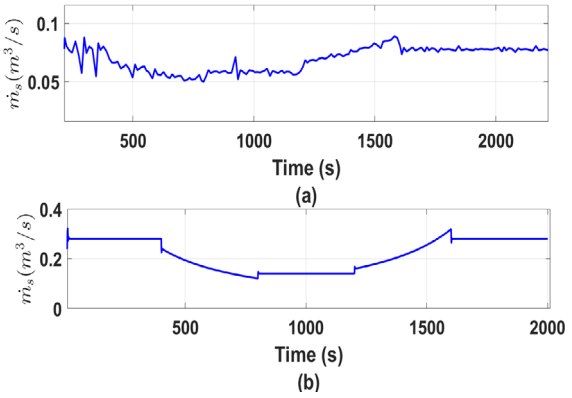

Figure 8. Supply air mass flow rate for (a) SMC, and (b) PID controllers

SMC is tracking the set point by applying less effort while PID applies more effort to reach the same set point at same time interval. Figure 9(a) shows the output tracking error for SMC and PID for temperature set point and Figure 9(b) shows the output tracking error for both controllers for CO2 set point.

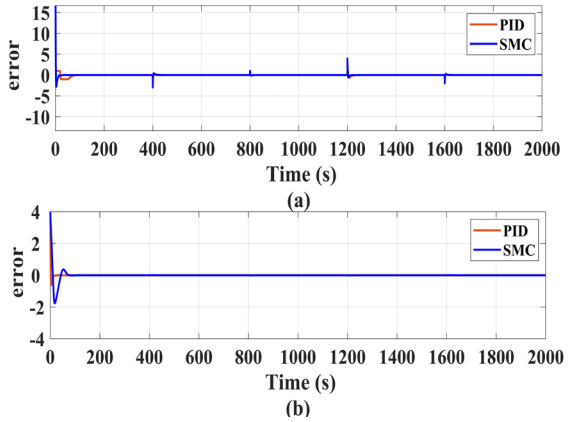

Figure 9. Output tracking error for both controllers for (a) Temperature set point and (b) $CO_{2\ set\ point}$

It is clear that despite the uncertainties the error converges to zero in a very short time when a change in set point occurs. SMC converges in a shorter time as compared to PID. Figure 10(a) and Figure 10(b) illustrate the fast convergence of sliding surfaces s_3 and s_1 respectively.

Performance indices are the criteria for measuring the efficiency of a controller. There are four performance indices, namely (a) Integral time absolute error (ITAE), (b) Integral time square error (ITSE), (c) Integral square error (ISE), and (d) Integral absolute error (IAE) for evaluating

the performance of a control system. Each error is calculated mathematically, it can be written as:

$$ISE = \int_0^\infty e(t)^2\,dt,$$
$$IAE = \int_0^\infty |e(t)|\,dt,$$
$$ITAE = \int_0^\infty t\,|e(t)|\,dt, \quad (23)$$
$$ITSE = \int_0^\infty te(t)^2\,dt,$$

where *t is time, e(t) is error, te(t)*2 is square of error multiplied by value of time.

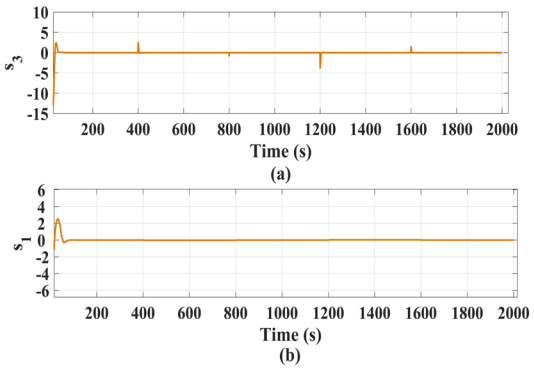

Figure 10. The fast convergence of the sliding surfaces (a) *s*3 for *u*1 and (b) *s*1 for *u*2

The calculated values for all four performance indices are illustrated in Table 3. For simplification purposes, multi-objective function is employed for calculating the average of all four errors, using (24):

$$F_{m.o} = \frac{ITSE + IAE + ITAE + ISE}{4} \quad (24)$$

The numerical vaules of the parameters considered for the tram thermal dynamic model are shown in Table 2. Figure 11(a) and Figure 11(b) show the performance indices of the multi-objective function (Fm.o) for both SMC and PID for the temperature set point and Co2 set point.

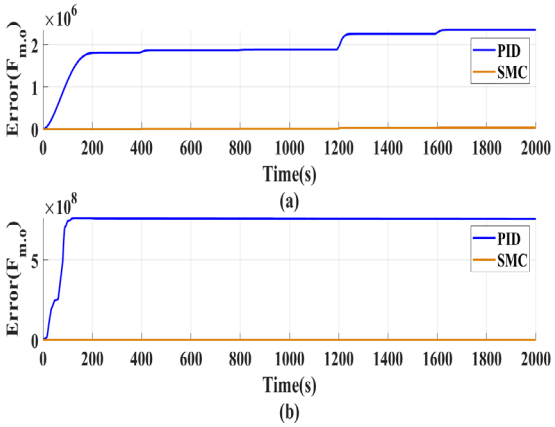

Figure 11. Multi-objective performance indices for both controllers for (a) Temperature set point and (b) c_{o2} set point

The controller with an output tracking error which is closer to zero is considered superior. SMC shows better convergence and values closer to zero.

Table 2. Numerical values of tram thermal dynamic model parameters

Parameter	Value	Unit
C_i	2.5	J/kgK
C_v	1.7x10^7	J/kgK
S	0.1	
T_o	5	°C
c_v	246	w/m^{2}K
c_{sol}	100	cm^{-1}
e_{sol}	1000	w/sr
C_p(t)	100	W
n_p	40	
C_a	3.2	J/kgK
V_i	6	m^3
d_i	1.29	Kg/m^3
n_{co2}	0.7	
γ_m	0.6	
co	800	ppm

Table 3. Numerical values of the four types of performance indices for both SMC and PID controllers

	Temperature		Co_2	
Error	**SMC**	**PID**	**SMC**	**PID**
IAE	49.69	2393	1706	3.893x10^4
ISE	267.8	3.123x10^4	5.711x10^5	1.878x10^7
ITAE	1.625x10^4	3.38x10^5	1.703x10^4	2.005x10^6
ITSE	1.728x10^4	1.98x10^6	6.182x10^5	7.336x10^8

5. Conclusion

Rail travel accounts for most of the total power utilization in the energy sector, and the HVAC is the second biggest user of energy in rail vehicles. Energy efficiency in HVACs needs proper control design due to its enhanced complexity. This paper describes all aspects of the thermal comfort in trams (tram HVAC and thermal comfort). A dynamic model of a tram and HVAC is considered, in which external disturbances (solar radiation and outside temperature) and model parametric uncertainties are included. Afterwards, two different control strategies namely: (a) a decoupled sliding mode control, and (b) a PID controller are applied for robust performance and efficiency of the HVAC system. Advanced sliding mode control is implemented for multi-input multi-output

(MIMO) thermal model of tram dynamics, which disintegrates the nonlinear MIMO system into two analogous single-input single-output (SISO) systems, while the uncertainties are also taken into account. The cabin temperature and concentration of Co2 are regulated by controlling the heater/ compressor power and the supply air mass flow rate. The inclusion of a sequence of steps function and ramp-step functions is meant for possible configuration of ideal cabin temperature and Co2 concentration level, respectively. The following generic findings are based on the results obtained:

1. SMC is more effective in monitoring various desired goals and in the presence of model uncertainties, it guarantees stability and robust performance;

2. To achieve the desired set point, SMC uses less power and a lower air mass flow rate;

3. In the convergence of output tracking error and sliding surface towards zero, SMC shows fast convergence. The performance indices and their related multi-objective function values are higher for SMC in comparison with PID.

REFERENCES

Alfieri, L., Battistelli, L. & Pagano, M. (2019). Impact on railway infrastructure of wayside energy storage systems for regenerative braking management: a case study on a real Italian railway infrastructure, *IET Electrical Systems in Transportation*, *9*(3), 140-149.

Aliahmadipour, M., Abdolzadeh, M. & Lari, K. (2017). Air flow simulation of HVAC system in compartment of a passenger coach, *Applied Thermal Engineering*, *123*, 97 -990.

Anon. (2019) *KULI Software*. Available at: <https://kuli.magna.com/index.php?id=33>, last accessed: May 11, 2021.

Beinarts, I. (2013). Fuzzy logic control method of HVAC equipment for optimization of passengers' thermal comfort in public electric transport vehiclesm In *Eurocon 2013* (pp. 1180-1186). IEEE.

Beusen, B., Degraeuwe, B. & Debeuf, P. (2013). Energy savings in light rail through the optimization of heating and ventilation, *Transportation Research Part D - Transport and Environment*, *23*, 50-54.

Bode, F., Nastase, I., Meslem, A. & Danca, P. (2017). The influence of the Inlet angle of vehicle air diffuser on the thermal comfort of passengers. In *2017 International Conference on Energy and Environment (CIEM)*, (pp. 442-446). IEEE.

Davies, G. F., Francis, C., Evans, J. A. & Maidment, G. G. (2017). Overview of Sustainable Refrigerated Road Transport Systems, *Reference Module in Food Science.* Elsevier.

Douglas, H., Roberts, C., Hillmansen, S. & Schmid, F. (2015). An assessment of available measures to reduce traction energy use in railway networks, *Energy Conversion and Management*, *106*, 1149 - 1165.

Dullinger, C., Struckl, W. & Kozek, M. (2015). A modular thermal simulation tool for computing energy consumption of HVAC units in rail vehicles, *Applied Thermal Engineering*, *78*, 616 - 629.

Fiori, C. & Marzano, V. (2018). Modelling energy consumption of electric freight vehicles in urban pickup/delivery operations: analysis and estimation on a real-world dataset, *Transportation Research Part D - Transport and Environment*, *65*, 658-673.

Gao, Z. & Yang, L. (2019). Energy-saving operation approaches for urban rail transit systems, *Frontiers of Engineering Management*, *6*(2), 139 - 151.

González-Gil, A., Palacin, R. & Batty, P. (2015). Optimal energy management of urban rail systems: Key performance indicators, *Energy Conversion and Management*, *90*, 282-291.

González-Gil, A., Palacin, R., Batty, P. & Powell, J., (2014). A systems approach to reduce urban rail energy consumption, *Energy Conversion and Management*, *80*, 509-524.

Hofstädter, R. N., Zero, T., Dullinger, C., Richter, G. & Kozek, M. (2017). Heat capacity and heat transfer coefficient estimation for a dynamic thermal model of rail vehicles, *Mathematical and Computer Modelling of Dynamical Systems*, *23*(5), 1-11.

Kim, J., Schiavon, S. & Brager, G. (2018). Personal comfort models - A new paradigm in thermal comfort for occupant-centric environmental control, *Building and Environment*, *132*, 114-124.

Konstantinov, M. & Wagner, C. (2015). Numerical simulation of the thermal comfort in train cabin, *International Journal of Railway Technology*, *4*(3), 69-88.

Kristanto, D. & Leephakpreeda, T. (2017). Energy Conversion for Thermal Comfort and Air Quality Within Car Cabin. In *IOP Conference Series: Materials Science and Engineering*, *187*(1), (p. 012037). IOP Publishing.

Krzaczek, M., Florczuk, J. & Tejchman, J. (2019). Improved energy management technique in pipe-embedded wall heating/cooling system in residential buildings, *Applied Energy*, *254*, 113711.

Lee, H., Hwang, Y., Song, I. & Jang, K. (2015). Transient thermal model of passenger car's cabin and implementation to saturation cycle with alternative working fluids, *Energy*, *90*, 1859-1868.

Li, Y.N. & Wang, Y. (2015). Study on control model of air-conditioning system of air-conditioned train in Qinghai-Tibet Railway, *Applied Mechanics and Materials, 713*, 905 - 908. Trans Tech Publications Ltd.

Lim, H. & Jeong, J.-W. (2019). Applicability and energy saving potential of thermoelectric radiant panels in high-speed train cabins, *International Journal of Refrigeration*, *104*, 229-245.

Lin, B. & Du, Z. (2017). Can urban rail transit curb automobile energy consumption, *Energy Policy*, *105*, 120 - 127.

Liu, J. & Wang, X. (2012). *Advanced sliding mode control for mechanical systems*, 31-35. Berlin, Springer.

Luchini, E., Schirrer, A., Jakubek, S. & Kozek, M. (2019). Model predictive multirate control for mixed-integer optimisation of redundant refrigeration circuits, *Journal of Process Control*, *76*, 112-121.

Luger, C., Kallinovsky, J. & Rieberer, R. (2016). Identification of representative operating conditions of HVAC systems in passenger rail vehicles based on sampling virtual train trips, *Advanced Engineering Informatics*, *30*(2), 157-167.

Luger, C. & Rieberer, R. (2018). Multi-objective design optimization of a rail HVAC CO2 cycle, *International Journal of Refrigeration*, *92*, 133-142.

Marcos, D., Pino, F. J., Bordons, C. & Guerra, J. J. (2014). The development and validation of a thermal model for the cabin of a vehicle, *Applied Thermal Engineering*, *66*(1-2), 646-656.

Mastrullo, R., Mauro, A. W. & Vellucci, C. (2016). Refrigerant alternatives for high speed train A/C systems: energy savings and environmental emissions evaluation under variable ambient conditions, *Energy Procedia*, *101*, 280-287.

Muhammad, R., Kamaruddin, M. K. & See, Y. P. (2018). Influence of Passenger Car Air Conditioner System Thermostat Level Setting to Fuel Consumption and Thermal Comfort, *Engineering Applications for New Materials and Technologies*, . 183-195. Springer, Cham.

Pero, F. D., Delogu, M., Pierini, M. & Bonaffini, D. (2015). Life Cycle Assessment of a heavy metro train, *Journal of Cleaner Production*, *87*, 787-799.

Rugh, J. P., Bennion, K., Brooker, A., Langewisch, J., Smith, K. & Meyer, J. (2011). PHEV/EV Integrated Vehicle Thermal Management-Development of a KULI Model to Assess Combined Cooling Loops, *Vehicle Thermal Management Systems Conference and Exhibition (VTMS10)*. National Renewable Energy Lab. (NREL), Golden, CO, United States. DOI: 10.1533/9780857095053.8.649

Shah, A., Huang, D., Chen, Y., Kang, X. & Qin, N. (2017). Robust sliding mode control of air handling unit for energy efficiency enhancement, *Energies*, *10*(11), 1815.

Shah, A., Huang, D., Huang, T. & Farid, U. (2018). Optimization of Buildings Energy Consumption by Designing Sliding Mode Control for Multizone VAV Air Conditioning Systems, *Energies*, *11*(11), 2911.

Suárez, C., Iranzo, A., Salva, J. A., Tapia, E., Barea, G. & Guerra, J. (2017). Parametric investigation using computational fluid dynamics of the HVAC air distribution in a railway vehicle for representative weather and operating conditions, *Energies*, *10*(8), 1074.

Talib, R., Nabil, N. & Choi, W. (2020). Optimization-based data-enabled modeling technique for HVAC systems components, *Buildings*, *10*(9), 163.

Velivelli, A., Guerithault, D. & Stöwe, S. (2017). Optimum seat cooling distribution for targeted human thermal comfort®, *SAE International Journal of Passenger Cars - Mechanical Systems*, *10*(1), 128-134.

Yang, B. & Wang, F. (2018). Supplementary opinions on alternative cooling technologies in hot climate, *International Journal of Biometeorology*, *62*(10), 1927-1928.

Zhang, Z., Liu, S. & Tian, L. (2011). Thermodynamic analysis of air cycle refrigeration system for Chinese train air conditioning, *Systems Engineering Procedia*, *1*, 1-22.